

Onset of Synchronization in Complex Networks of Noisy Oscillators

Bernard Sonnenschein* and Lutz Schimansky-Geier

Department of Physics, Humboldt-Universität zu Berlin,

Newtonstr. 15, 12489 Berlin, Germany; and

Bernstein Center for Computational Neuroscience Berlin, Philippstr. 13, 10115 Berlin, Germany

We study networks of noisy phase oscillators whose nodes are characterized by a random degree counting the number of its connections. Both these degrees and the natural frequencies of the oscillators are distributed according to a given probability density. Replacing the randomly connected network by an all-to-all coupled network with weighted edges, allows us to formulate the dynamics of a single oscillator coupled to the mean field and to derive the corresponding Fokker-Planck equation. From the latter we calculate the critical coupling strength for the onset of synchronization as a function of the noise intensity, the frequency distribution and the first two moments of the degree distribution. Our approach is applied to a dense small-world network model, for which we calculate the degree distribution. Numerical simulations prove the validity of the made replacement. We also test the applicability to more sparsely connected networks and formulate homogeneity and absence of correlations in the degree distribution as limiting factors of our approach.

PACS numbers: 05.40.-a, 05.45.Xt, 87.10.Ca, 87.19.lj

I. INTRODUCTION

Synchronization phenomena have been observed in many different fields such as the chaotic intensity fluctuations of coupled lasers [1], flashing swarms of fireflies [2], spiking dynamics of neurons [3–6], pacemaker cells in the heart [7], and the menstrual cycles of women living together [8–10], to mention only a few examples. Without doubts, the phenomenon of synchronization is a central mechanism in physics, chemistry, biology, and medicine as reported impressively in various monographs [11–14].

The key aspect of our analysis is the phase description of the dynamics [15]. With regard to biological oscillators, the idea of the phase description goes back to Winfree (1967) who motivated it by the observation that the oscillators should be weakly coupled so that no oscillator is ever perturbed far away from its limit cycle and therefore amplitudes could be considered as fixed [16].

Kuramoto (1975, 1984) simplified the Winfree model by certain methods of perturbation and averaging [17, 18]. The Kuramoto model has been shown to be a very successful approach to the problem of synchronization [19]. By virtue of its simplicity the Kuramoto model is analytically tractable. We take advantage of the simplicity to the greatest extent, but at the same time we are determined to make the model more realistic, in particular with regard to neural networks. Therefore, we add two features: (i) we consider complex networks instead of all-to-all connectivity and (ii) we study noise in the phase model. The first feature takes account of the fact that many real-world networks, such as neural systems, are complex networks “par excellence” [20], while the second feature incorporates experimentally observed stochastic processes, such as the random synaptic inputs from other neurons [15].

*Electronic address: sonne@physik.hu-berlin.de

For an ensemble of Kuramoto oscillators, both features have been considered separately in the literature: complex networks in [21–23] and noise in [24–26]. For an overview on nonlinear dynamics in complex networks we recommend [27–30] and for an overview on the Kuramoto model we further recommend [31–33].

Referring to [22], we apply an approximation technique, in which we focus on the degrees of the nodes, i.e. the numbers of connections leading to and emanating from a node. The degree distribution could be given “a priori” and then defines the network or it is determined by counting the frequencies of the edges for every node of the large network under consideration.

As a result of the approximation, the complex network is replaced by an all-to-all coupled one with weighted edges, which mimics the original complex structure. This procedure originates a mean-field like description that enables us to derive both the effective Langevin equation for a single oscillator inside the random network and the corresponding nonlinear Fokker-Planck equation (FPE). Moreover, the latter gives us the possibility to calculate the critical coupling strength that marks the onset of synchronization in the network.

The work is organized as follows. In section II we present our extended Kuramoto model and in section III we explain the approximation technique. In section IV we derive the nonlinear FPE and in V the critical coupling strength. This result is compared with numerical simulations on small-world networks (section VI), and the applicability to other networks is discussed (section VII). In the last section VIII we give concluding remarks.

II. CONCEPTION OF OUR MODEL

We refer to the original Kuramoto model [17, 18] in the following way:

$$\dot{\phi}_i(t) = \omega_i + \frac{\varkappa}{N} \sum_{j=1}^N A_{ij} \sin(\phi_j(t) - \phi_i(t)) + \xi_i(t), \quad i = 1, \dots, N, \quad (1)$$

with the number of oscillators N , the phase $\phi_i(t)$ at time t and natural frequency ω_i of oscillator i . The coupling strength is denoted by \varkappa and A_{ij} are the elements of the adjacency matrix. If the nodes i and j are not connected, then $A_{ij} = 0$, otherwise $A_{ij} = 1$. Self-coupling is excluded in weighted networks. The adjacency matrix further yields the individual degrees:

$$k_i = \sum_{j=1}^N A_{ij}, \quad i = 1, \dots, N. \quad (2)$$

The natural frequencies and individual degrees are distributed according to a joint probability density $P(\omega, k)$.

Remember that the indegree or the outdegree of node i are defined as the number of edges pointing to or emanating from node i , respectively [34]. Since we consider undirected networks, the adjacency matrix is symmetric and the indegrees are equal to the outdegrees. Hence, we refer only to the degree k_i of node i .

The division by N in the coupling term of Eq. (1) is not always the correct normalization for complex networks, because it might not lead necessarily to an intensive coupling term. That is the case, if the adjacency matrix does not scale with the system size. Then one has to take the maximum degree instead [30].

The functions $\xi_i(t)$, $i = 1, \dots, N$, stand for sources of independent white noise processes that act on the natural frequencies as a stochastic force. They satisfy

$$\begin{aligned} \langle \xi_i(t) \rangle &= 0, \\ \langle \xi_i(t) \xi_j(t') \rangle &= 2D \delta_{ij} \delta(t - t'). \end{aligned} \quad (3)$$

Hence, a single nonnegative parameter D scales the noise. It is its intensity and we assume that it is independent of the system size. The angular brackets denote an average over different realizations of the noise.

III. APPROXIMATION TECHNIQUE

The idea is to adopt a combinatorial point of view in order to mimic the complex network by a weighted fully connected network with a new adjacency matrix \tilde{A}_{ij} which should resemble the original structure defined by the given set of degrees k_i , $i = 1, \dots, N$. We require that the approximating weights \tilde{A}_{ij} conserve the degrees of the original network (cf. Eq. (2)), i.e.

$$k_i \stackrel{!}{=} \sum_{j=1}^N \tilde{A}_{ij} \quad \text{and} \quad k_j \stackrel{!}{=} \sum_{i=1}^N \tilde{A}_{ij}, \quad (4)$$

where we assume again an undirected network. Eq. (4) also means that the new matrix scales in the same way as the old one, if the system size is changed.

In order to construct the approximating weight between nodes i and j , we treat the original complex network as a random network and assume that the coupling strength is proportional to the probability that a node with degree k_i couples to a node with degree k_j . If the degrees are uncorrelated [22, 35], then \tilde{A}_{ij} is equal to the degree k_i times the degree k_j normalized by the total number of all degrees in the network:

$$\tilde{A}_{ij} = k_i \frac{k_j}{\sum_{l=1}^N k_l}. \quad (5)$$

Obviously, it defines a symmetric matrix since the same expression is found using the same arguments for the weight of the edge connecting the j -th with the i -th node. It is easy to see that the new matrix conserves the local degree structure as required in Eq. (4) and the scaling of the adjacency matrix. We illustrate our approximation in Fig. 1.

Inserting Eq. (5) into Eq. (1) yields

$$\dot{\phi}_i(t) = \omega_i + \frac{\varkappa}{N} \frac{k_i}{\sum_{l=1}^N k_l} \sum_{j=1}^N k_j \sin(\phi_j(t) - \phi_i(t)) + \xi_i(t), \quad i = 1, \dots, N. \quad (6)$$

This is the approximative form of our model, which appears to be analytically tractable.

Let us make the following definition (cf. Ref. [22]):

$$r(t) e^{i\Theta(t)} := \frac{\sum_{j=1}^N k_j e^{i\phi_j(t)}}{\sum_{j=1}^N k_j}. \quad (7)$$

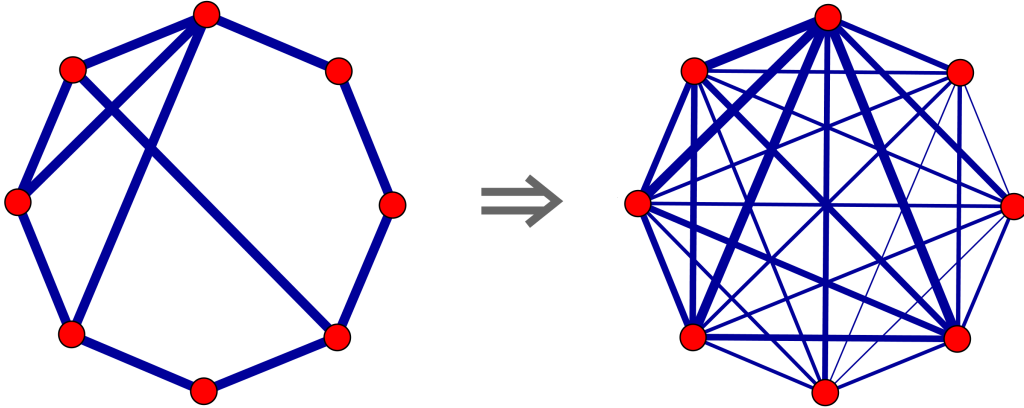


FIG. 1: (Color online) The effect of our approximation on a ring network of eight symmetrically coupled oscillators. On the left-hand side the original complex network is shown and on the right-hand side the approximate network is shown, where the thickness of the edges is chosen approximately proportional to the coupling strength. For reasons of clarity, self-coupling is not visualized.

The quantity $r(t)$ is an order parameter, because for a population of $N \rightarrow \infty$ completely asynchronous oscillators, $r(t \rightarrow \infty)$ vanishes, while the onset of synchronization is marked by $r(t \rightarrow \infty) > 0$ (the completely phase synchronized state corresponds to $r(t \rightarrow \infty) = 1$).

By multiplying Eq. (7) by $e^{-i\phi_i(t)}$ and by considering only the imaginary parts, we can rewrite Eq. (6) as an effective one-oscillator description, where the common time-dependent phase $\Theta(t)$ and amplitude $r(t)$ are averaged over all the nodes according to Eq. (7):

$$\dot{\phi}_i(t) = \omega_i + r(t)\kappa \frac{k_i}{N} \sin(\Theta(t) - \phi_i(t)) + \xi_i(t), \quad i = 1, \dots, N. \quad (8)$$

In other words, our approximation is equivalent to a mean-field approximation with the mean field amplitude $r(t)$ and phase $\Theta(t)$ defined in Eq. (7). All oscillators are statistically identical and differ by ω_i and k_i only. They are coupled to the mean field with a characteristic strength that is proportional to the individual degree k_i , which can be seen as a property of node i . Such an assignment is similar to a characterization of subpopulations through coupling strengths [36].

IV. DERIVATION OF THE NONLINEAR FOKKER-PLANCK EQUATION

The solution of the system of N coupled Langevin equations in Eq. (6) is a Markov process. It can also be formulated by the help of the transition probability $\mathcal{P}(\boldsymbol{\phi}, t | \boldsymbol{\phi}^0, t^0; \boldsymbol{\omega}, \mathbf{k})$ that describes the evolution of the phases from time t^0 to time $t > t^0$. Therein, respectively the vector $\boldsymbol{\phi} = (\phi_1, \dots, \phi_N)$ contains the phases of the N oscillators at time t and $\boldsymbol{\phi}^0 = (\phi_1^0, \dots, \phi_N^0)$ at initial time t^0 . The vectors $\boldsymbol{\omega} = (\omega_1, \dots, \omega_N)$ and $\mathbf{k} = (k_1, \dots, k_N)$ contain the natural frequencies of the oscillators and the degrees of all the nodes in the network, respectively. The individual frequencies $\boldsymbol{\omega}$ and degrees \mathbf{k} are initially chosen at time $t = t^0$ and they stay fixed during the whole evolution. We also assume that the initial phases ϕ_i^0 are identically and independently distributed.

The transition probability $\mathcal{P}(\boldsymbol{\phi}, t | \boldsymbol{\phi}^0, t^0; \boldsymbol{\omega}, \mathbf{k})$ for N oscillators satisfies a linear Fokker-Planck

equation (FPE)

$$\frac{\partial \mathcal{P}}{\partial t} = - \sum_i \frac{\partial}{\partial \phi_i} \left(\omega_i \mathcal{P} + k_i \frac{\varkappa}{N} \sum_{j=1}^N \frac{k_j}{\sum_{l=1}^N k_l} \sin(\phi_j - \phi_i) \mathcal{P} \right) + D \sum_i \frac{\partial^2 \mathcal{P}}{\partial \phi_i^2} \quad (9)$$

and is subject to the initial condition

$$\mathcal{P}(\boldsymbol{\phi}, t^0 | \boldsymbol{\phi}^0, t^0; \boldsymbol{\omega}, \mathbf{k}) = \delta^N(\boldsymbol{\phi} - \boldsymbol{\phi}^0). \quad (10)$$

Conditioned and joint probabilities satisfy

$$\mathcal{P}(\boldsymbol{\phi}, t | \boldsymbol{\phi}^0, t^0; \boldsymbol{\omega}, \mathbf{k}) \mathcal{P}(\boldsymbol{\phi}^0, t^0; \boldsymbol{\omega}, \mathbf{k}) = \mathcal{P}(\boldsymbol{\phi}, t; \boldsymbol{\omega}, \mathbf{k} | \boldsymbol{\phi}^0, t^0) \mathcal{P}(\boldsymbol{\phi}^0, t^0). \quad (11)$$

As already stated in section II, the natural frequencies and degrees are distributed according to the joint probability density $P(\omega, k)$. The initial phases of the oscillators are further supposed to be chosen independently of $\boldsymbol{\omega}$ and \mathbf{k} . Therefore, we have the joint distribution of initial phases, edges and frequencies at initial time t^0 factorizing as

$$\mathcal{P}(\boldsymbol{\phi}^0, t^0; \boldsymbol{\omega}, \mathbf{k}) = \prod_{i=1}^N P(\omega_i, k_i) \mathcal{P}(\phi_i^0, t^0). \quad (12)$$

The joint distribution at a later time t becomes independent of the initial distribution by integrating Eq. (11) over the initial phases:

$$\mathcal{P}(\boldsymbol{\phi}, t; \boldsymbol{\omega}, \mathbf{k}) = \int d\phi_1^0 \dots d\phi_N^0 \mathcal{P}(\boldsymbol{\phi}, t | \boldsymbol{\phi}^0, t^0; \boldsymbol{\omega}, \mathbf{k}) \prod_{i=1}^N P(\omega_i, k_i) \mathcal{P}(\phi_i^0, t^0). \quad (13)$$

Again, we aim at reducing the description to an effective one-oscillator picture. As does the transition probability, the distribution Eq. (13) obeys the FPE (9). A reduced joint distribution ρ_n with $n < N$ for n phases with frequencies $\omega_1 \dots \omega_n$ and degrees k_1, \dots, k_n is defined in the usual way [37]:

$$\begin{aligned} \rho_n(\phi_1, \dots, \phi_n, t; \omega_1, \dots, \omega_n, k_1, \dots, k_n) \\ := \int d\phi_{n+1} \dots d\phi_N \int d\omega_{n+1} \dots d\omega_N \int dk_{n+1} \dots dk_N \mathcal{P}(\boldsymbol{\phi}, t; \boldsymbol{\omega}, \mathbf{k}). \end{aligned} \quad (14)$$

For the important case of a single oscillator $n = 1$ imbedded in the network, we integrate Eq. (9) over the remaining $N - 1$ phases (ϕ_2, \dots, ϕ_N) , frequencies $(\omega_2, \dots, \omega_N)$ and degrees (k_2, \dots, k_N) :

$$\begin{aligned} \frac{\partial \rho_1}{\partial t} = - \frac{\partial}{\partial \phi_1} \omega_1 \rho_1 + D \frac{\partial^2 \rho_1}{\partial \phi_1^2} - \\ - \frac{\partial}{\partial \phi_1} \left[\frac{\varkappa}{N} \frac{k_1 (N-1)}{\sum_l k_l} \int d\phi_2 \int d\omega_2 \int dk_2 \sin(\phi_2 - \phi_1) k_2 \rho_2(\phi_1, \phi_2, t; \omega_1, \omega_2, k_1, k_2) \right], \end{aligned} \quad (15)$$

where we use identity of all the oscillators in the statistical sense. As a result the binary interaction of the phase oscillators looks in the usual way and relates hierarchically to reduced probabilities with a larger number $n > 2$. However, the interaction appears as averaged over the frequency-degree distribution (cf. Eq. (20)).

In the thermodynamic limit $N \rightarrow \infty$ the ratio $\sum_l k_l / (N - 1)$ becomes the average degree. Moreover, the correlation of phases between any two oscillators can be discarded [37] within the scope of the mean-field approximation, Eq. (6):

$$\rho_2(\phi_1, \phi_2, t; \omega_1, \omega_2, k_1, k_2) = \rho_1(\phi_1, t; \omega_1, k_1) \rho_1(\phi_2, t; \omega_2, k_2). \quad (16)$$

Such a decoupling has also been used in [22, 23, 35, 38] and it is an omnipresent approximation in the theory of phase transitions [39]. A completely rigorous discussion about the general conditions has been proposed in [33] by the help of path integral methods. We point out that this effective decoupling is fully equivalent to the former description by the help of the stochastic differential equation for the single phase oscillator imbedded in the mean field (cf. Eq. (8)).

Let us return to the conditional probability density

$$\rho_1(\phi_1, t | \omega_1, k_1) = \frac{\rho_1(\phi_1, t; \omega_1, k_1)}{P(\omega_1, k_1)}, \quad (17)$$

by which we get eventually a nonlinear Fokker-Planck equation for the one-oscillator probability density ρ_1 :

$$\frac{\partial \rho_1(\phi_1, t | \omega_1, k_1)}{\partial t} = - \frac{\partial}{\partial \phi_1} [v(\phi_1, t) \rho_1(\phi_1, t | \omega_1, k_1)] + D \frac{\partial^2 \rho_1(\phi_1, t | \omega_1, k_1)}{\partial \phi_1^2}. \quad (18)$$

Therein the mean increment of the phase per unit time reads

$$v(\phi_1, t) = \omega_1 + r \tilde{\varkappa} k_1 \sin(\Theta - \phi_1). \quad (19)$$

It depends on the density $\rho_1(\phi_1, t | \omega_1, k_1)$ via the order parameter

$$r e^{i\Theta} = \frac{1}{\langle k \rangle} \int_0^{2\pi} d\phi_2 \int_{-\infty}^{+\infty} d\omega_2 \int_m^{\infty} dk_2 e^{i\phi_2} \rho_1(\phi_2, t | \omega_2, k_2) k_2 P(\omega_2, k_2). \quad (20)$$

Here $\tilde{\varkappa} := \varkappa / N$ and $m \geq 1$ is the lowest possible degree in our network. Eqs. (18)-(20) constitute again an effective one-oscillator description as Eqs. (7), (8). Both descriptions are equivalent for all possible pairs ω_i and k_i , the difference is that in this section the equations are derived for the thermodynamic limit. We remark that our expressions are reminiscent of the equations in the work of Ichinomiya [22], who considers uncorrelated random networks without noise. We emphasize that the above averaging requires a coarse grained statistical approach to all the nodes. Since each of the N oscillators is coupled to the mean field with a characteristic strength, we refer to the “weighted mean field”, which makes sense if the initial conditions of all oscillators are identically distributed. We also note that the conditional probability density $\rho_1(\phi_1, t | \omega_1, k_1)$ in Eq. (17) is averaged over the initial conditions. If one would formulate the theory for the transition probability $\rho_1(\phi_1, t | \phi^0, t^0, \omega_1, k_1)$ the nonlinear FPE (18) would be the same. A difference would occur in the definition of the order parameter, where one has to remember that the definition (20) includes the average over the initial conditions as it was performed in Eq. (12).

V. THE CRITICAL COUPLING STRENGTH

To underline the statistical identity of the oscillators in the one-oscillator description, we omit the indices and proceed with variables ϕ, ω, k . Taking into account the normalization condition

$$\int_0^{2\pi} \rho(\phi, t | \omega, k) d\phi = 1, \quad \forall \omega, k, t, \quad (21)$$

the completely asynchronous stationary state is given by

$$\rho_0(\phi|\omega, k) = \frac{1}{2\pi} = \text{const.}, \quad \forall \omega, k, t \quad (22)$$

with order parameter $r = r_0 = 0$ and undefined phase. It is easy to see that ρ_0 is at least one of the possible asymptotic solutions of the nonlinear FPE (20).

In the following, we will perform a linear stability analysis of this incoherent solution. In doing so, we refer to the work of Strogatz and Mirollo [25], who also study a nonlinear FPE in order to investigate the linear stability of the incoherent state for an unweighted all-to-all connectivity. The critical condition, where the incoherent solution loses its stability, is equivalent to the onset of synchronization we are searching for. To start with, we consider the evolution of a small perturbation of the incoherent state:

$$\rho(\phi, t|\omega, k) = \frac{1}{2\pi} + \epsilon \delta\rho(\phi, t|\omega, k), \quad \epsilon \ll 1. \quad (23)$$

The normalization condition (21) implies

$$\epsilon \int_0^{2\pi} \delta\rho(\phi, t|\omega, k) d\phi = 0 \quad \forall \omega, k, t, \quad (24)$$

so $\delta\rho(\phi, t|\omega, k)$ is 2π -periodic in ϕ . Now we substitute Eq. (23) into Eq. (18),

$$\epsilon \frac{\partial \delta\rho}{\partial t} = -\frac{\partial}{\partial \phi} \left[\left(\frac{1}{2\pi} + \epsilon \delta\rho \right) v \right] + \epsilon D \frac{\partial^2 \delta\rho}{\partial \phi^2}. \quad (25)$$

The amplitude becomes $r(t) = \epsilon \delta r(t)$, where $\delta r(t)$ is given by substituting ρ by $\delta\rho$ in Eq. (20). The FPE (18) linearized in the lowest order in ϵ then reads

$$\frac{\partial \delta\rho}{\partial t} = -\omega \frac{\partial \delta\rho}{\partial \phi} + \frac{\tilde{z}k}{2\pi} \delta r \cos(\Theta - \phi) + D \frac{\partial^2 \delta\rho}{\partial \phi^2}. \quad (26)$$

Since $\delta\rho$ is a real number and 2π -periodic in ϕ (cf. Eq. (24)), it may be expanded as

$$\delta\rho(\phi, t|\omega, k) = \frac{1}{2\pi} \sum_{l=1}^{\infty} \{ c_l(t|\omega, k) e^{il\phi} + c_l^*(t|\omega, k) e^{-il\phi} \}. \quad (27)$$

Due to Eq. (24), $c_0(t|\omega, k)$ vanishes. The first nonvanishing coefficients, which constitute the so-called fundamental mode, determine the deviations of the mean field in first order of small ϵ :

$$\delta r e^{i\Theta} = \frac{1}{\langle k \rangle} \int_{-\infty}^{+\infty} d\omega' \int_m^{\infty} dk' c_1^*(t|\omega', k') k' P(\omega', k'). \quad (28)$$

In order that the incoherent state becomes unstable and a synchronization process starts, $c_1(t|\omega, k)$ has to grow, so that as a consequence the order parameter $r(t)$ grows as well.

Multiplication of the last equation by $e^{-i\phi}$ and considering only the real parts, yields

$$\delta r \cos(\Theta - \phi) = \frac{1}{2\langle k \rangle} \left(\int_{-\infty}^{+\infty} d\omega' \int_m^{\infty} dk' c_1(t|\omega', k') k' P(\omega', k') \right) e^{i\phi} + \text{c. c.} \quad (29)$$

Now we insert Eqs. (27)-(29) into Eq. (26) and consider only the coefficients with $e^{i\phi}$. Afterwards, one finds the evolution equation for the fundamental mode $c_1(t|\omega, k)$:

$$\frac{\partial c_1}{\partial t} = -(D + i\omega)c_1 + \frac{\tilde{\chi}k}{2\langle k \rangle} \int_{-\infty}^{+\infty} d\omega' \int_m^{\infty} dk' c_1(t|\omega', k') k' P(\omega', k') . \quad (30)$$

Since this is a partial differential equation without mixed derivatives, we make a separation ansatz:

$$c_1(t|\omega, k) \equiv b(\omega, k) e^{\lambda t}, \quad \lambda \in \mathbb{C}. \quad (31)$$

So we obtain

$$\lambda b = -(D + i\omega)b + \frac{\tilde{\chi}k}{2\langle k \rangle} \int_{-\infty}^{+\infty} d\omega' \int_m^{\infty} dk' b(\omega', k') k' P(\omega', k') . \quad (32)$$

The right-hand side is a linear transformation and it can be shown that we only have to calculate its point spectrum in order to obtain the critical coupling strength [25].

The second term on the right-hand side of Eq. (32) equals the degree k times a constant which we call B in the following, so that $b(\omega, k)$ is given by

$$b(\omega, k) = \frac{B \cdot k}{\lambda + D + i\omega} . \quad (33)$$

Hence, we can set up the following self-consistent equation:

$$B = \frac{\tilde{\chi}}{2\langle k \rangle} \int_{-\infty}^{+\infty} d\omega' \int_m^{\infty} dk' \frac{B \cdot k'^2}{\lambda + D + i\omega'} P(\omega', k') . \quad (34)$$

This relation holds, if all the oscillators are identical in the statistical sense, see section IV. We remark that Restrepo, Ott and Hunt (2005) derived a similar formula where fluctuations emerge due to finite-size effects [23]. We have defined in Eq. (3) the value D . As outlined, it does not vanish in the thermodynamic limit. In Eq. (34) the first integral exists for all $\text{Re}(\lambda) > -D$ [32]. The solution $B = 0$ is not allowed, because otherwise $b(\omega, k)$ and as a consequence $c_1(t|\omega, k)$ would vanish. $c_1(t|\omega, k) = 0$ however is not considered as an eigenfunction (it is a trivial solution). So B is canceled out and we get

$$1 = \frac{\tilde{\chi}}{2\langle k \rangle} \int_{-\infty}^{+\infty} d\omega' \int_m^{\infty} dk' \frac{k'^2}{\lambda + D + i\omega'} P(\omega', k') . \quad (35)$$

On the analogy of the proof in [40], one can show that there exists only one solution for λ and that it has to be a real number. The proof makes use of the assumption that, with regard to the ω -dependency, $P(\omega, k)$ has a single maximum at frequency $\omega = 0$ (due to the rotational symmetry in the model the maximum can be located like this) and is symmetric.

In summary the eigenvalue λ is given by

$$1 = \frac{\tilde{\chi}}{2\langle k \rangle} \int_{-\infty}^{+\infty} d\omega' \int_m^{\infty} dk' \frac{(\lambda + D) \cdot k'^2}{(\lambda + D)^2 + \omega'^2} P(\omega', k') . \quad (36)$$

Note that this equation can only be fulfilled if $\lambda > -D$, because otherwise the right-hand side would be nonpositive. Thus, the eigenvalue λ is strictly positive and the incoherent solution cannot be linearly stable, if the noise intensity vanishes.

At the critical condition $\lambda = \lambda_c = 0$ the incoherent solution loses its stability: if $\lambda > 0$ the fundamental mode c_1 of the perturbation $\delta\rho$ of the incoherent solution is linearly unstable. It grows exponentially with time $\sim e^{\lambda t}$ and so does the order parameter $r(t)$ (cf. Eq. (28)). Hence, the critical coupling strength \varkappa_c for the onset of synchronization reads

$$\varkappa_c = 2N\langle k \rangle \left[\int_{-\infty}^{+\infty} d\omega' \int_m^{+\infty} dk' \frac{D \cdot k'^2}{D^2 + \omega'^2} P(\omega', k') \right]^{-1}. \quad (37)$$

We emphasize that this equation is not valid in the noise-free case, where one has to take the limit $\lambda \rightarrow 0^+$ in Eq. (36) with $D = 0$, by which previous results can be reproduced [22, 23] (compare Tab. I).

In [41] we investigate the effects of correlations between the degrees k and the frequencies ω . Here we continue with two separated distributions $g(\omega)$ and $P(k)$. It is interesting to see that the critical coupling strength \varkappa_c can then be written as a product of two functionals. The first one maps the degree distribution $P(k)$ to a real number via the first two moments,

$$f_{\text{top}}[P] := N \frac{\langle k \rangle}{\langle k^2 \rangle}. \quad (38)$$

We call this one the “topology functional”. The second one maps the frequency distribution $g(\omega)$ to a real number via an integral that depends on the noise intensity D ,

$$f_{\text{div}}(D)[g] := 2 \left[\int_{-\infty}^{+\infty} \frac{D}{D^2 + \omega'^2} g(\omega') d\omega' \right]^{-1}. \quad (39)$$

We call this one the “diversity functional”. In short:

$$\varkappa_c = f_{\text{top}}[P] \cdot f_{\text{div}}(D)[g]. \quad (40)$$

VI. APPLICATION TO A DENSE SMALL-WORLD NETWORK MODEL

In this section we test the analytical expression for the critical coupling strength as a function of diversity, noise and network topology for local ring-like networks, where random shortcuts to other nodes will be established. For this purpose, we compare the analytical result with numerical simulations of networks with different size N .

A. Derivation of the Topology Function

First, we specify our dense small-world network model. According to the definition in [42], in dense networks of N nodes the total number of edges scales with N^2 . Our dense small-world networks are constructed as follows. Each oscillator is coupled to its K next neighbors in both directions of the ring network and K is given by

$$K = \left\lfloor \frac{\alpha}{2}(N-1) \right\rfloor, \quad 0 \leq \alpha \leq 1. \quad (41)$$

Here the intensive variable α gives the fraction of all nodes that are coupled through next neighbor connections. $\alpha = 0$ stands for uncoupled nodes, whereas in case of $\alpha = 1$ the network is fully

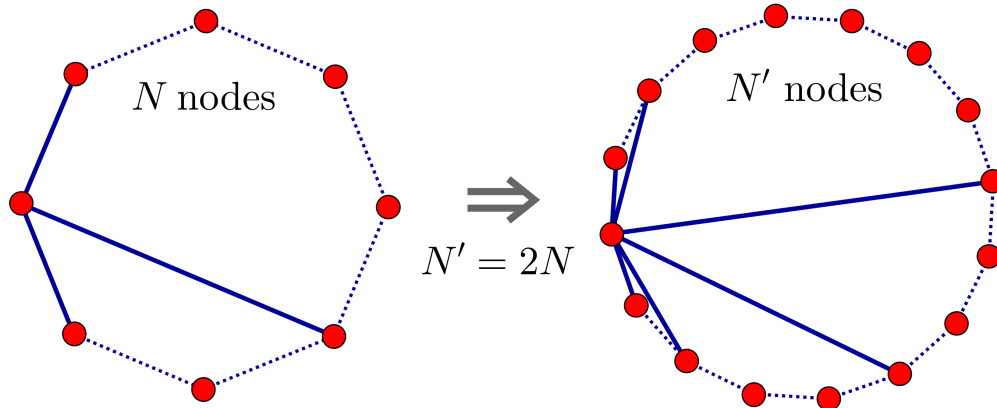


FIG. 2: (Color online) Visualization of a dense small-world network model. If the system size N is duplicated, the average number of connections is duplicated as well. The figure shows one marked node in the network.

connected. We underline that the variance of α vanishes. The floor function $\lfloor \cdot \rfloor$ gives the greatest integer less than or equal to its argument, by which the continuous variable α is mapped to the discrete variable K . So far we obtain a regular network and due to self-coupling, the fixed degree in such regular networks is $2K + 1$. The corresponding degree distribution is equal to the Kronecker symbol

$$P_{\text{local}}(k) = \delta_{k,2K+1} . \quad (42)$$

In our final simulations we choose $\alpha = 0.05$. Hence, 2.5 percent of possible edges are local regular connections.

Besides these $(2K + 1) \cdot N$ next neighbor couplings we introduce shortcuts: each oscillator is coupled to the remaining other $N - 2K - 1$ ones with a certain probability p (see Fig. 2 for illustration). If K equals zero the model generates Erdős-Rényi random networks. The case $p = 1$ leads to all-to-all connectivity other than in popular sparse small-world network models [43, 44]. The procedure of adding shortcuts can be seen as a Bernoulli experiment with probability p of success [27–29], so that the degree distribution $P(k)$ is given by the following binomial distribution:

$$P(k) = \binom{N - 2K - 1}{k - 2K - 1} p^{k - 2K - 1} [1 - p]^{N - k} , \quad k > 2K . \quad (43)$$

Note that the minimum degree $k = 2K + 1$ corresponds to Eq. (42). The first moment equals

$$\langle k \rangle = 2K + 1 + (N - 2K - 1)p \approx (N - 1)(\alpha + p - \alpha p) + 1 . \quad (44)$$

In the last step we have used Eq. (41) by neglecting the floor function as an approximation. For large N the latter expression approaches $\langle k \rangle \approx N(\alpha + p - \alpha p)$.

By simple substitutions one finds the second moment

$$\langle k^2 \rangle = \langle k \rangle^2 + (\langle k \rangle - 2K - 1)(1 - p) , \quad (45)$$

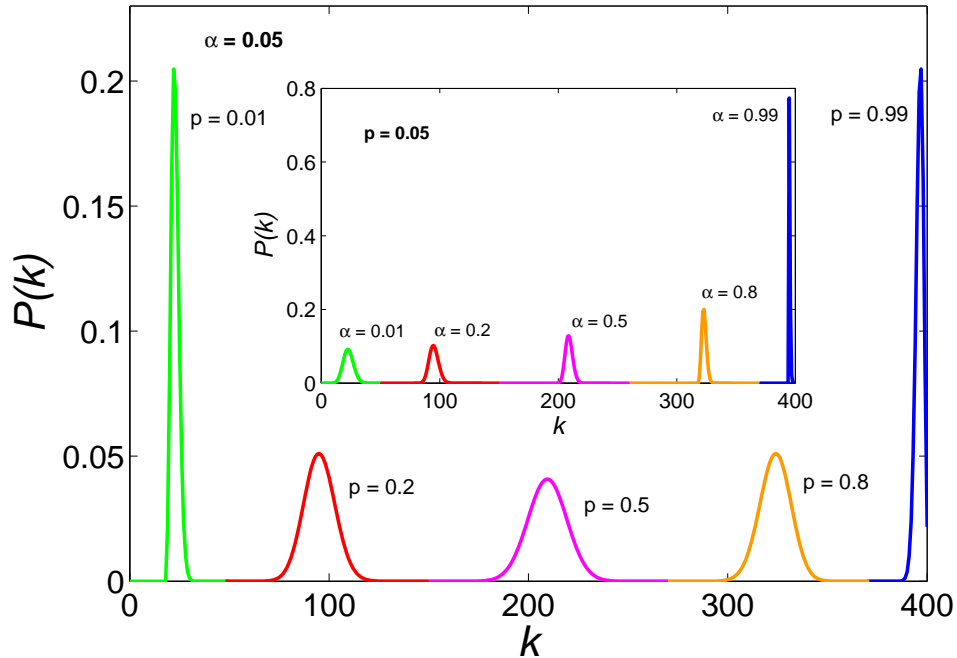


FIG. 3: (Color online) Degree distribution $P(k)$ of dense small-world networks consisting of 400 nodes depicted for different shortcut probabilities p and fractions of regular connections α (inset). For the sake of clarity solid lines are chosen.

where the second item equals the variance of k in the binomial distribution due to the randomness of the number of shortcuts. It scales only linearly with the system size, whereas the first item grows with N^2 . Thus, for large systems the difference between the nonrandom number of local connections and the number of shortcuts disappears, because the variability of the shortcuts does not count for large N . The second moment approaches $\langle k \rangle^2$ and it becomes symmetric in α and p . Hence, the topology function (cf. Eq. (38)) for large N results in

$$f_{\text{top}}(p, \alpha)|_{N \gg 1} \approx \frac{N}{\langle k \rangle} \approx \frac{1}{\alpha + p - \alpha p}. \quad (46)$$

We obtain as limiting cases (compare Fig. 4)

$$f_{\text{top}}(p, \alpha)|_{N \gg 1} \approx \begin{cases} \frac{1}{\alpha} + \frac{\alpha-1}{\alpha^2}p + O(p^2), & p \ll 1, \\ 2 - \alpha + (\alpha - 1)p + O((1-p)^2), & p \lesssim 1. \end{cases} \quad (47)$$

Due to the symmetry, we obtain qualitatively the same for $\alpha \ll 1$ and $\alpha \lesssim 1$, but with p and α being interchanged. As expected, the topology function tends to unity for $p \rightarrow 1$ or $\alpha \rightarrow 1$, because in both cases the network becomes fully connected.

In Fig. 4 the dependence of the topology function on α and p is depicted. Discrepancies between numerical calculations and theory in the right panel are due to the fact that the number of coupled

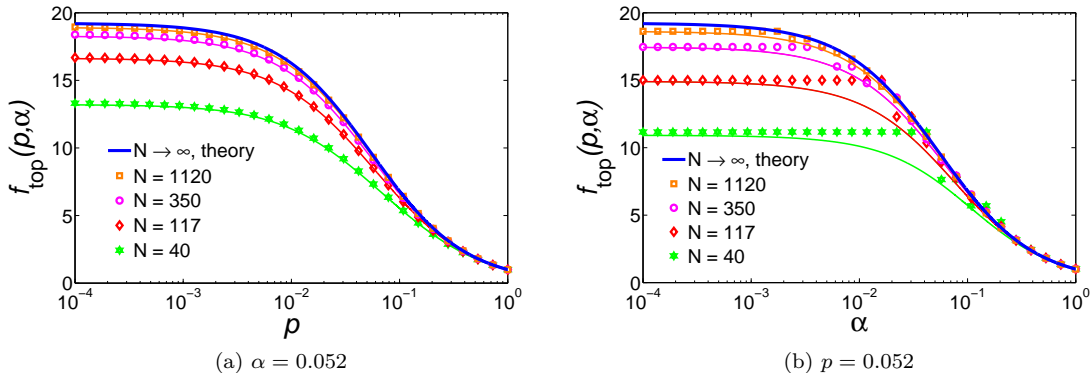


FIG. 4: (Color online) Dependency of the topology function on the system size N : Solid lines are given by the theory. The thick line corresponds to the thermodynamic limit and slight lines are calculated according to Eqs. (44) and (45) for smaller systems. Markers show results of numerical calculations for indicated system sizes.

next neighbors is, of course, an integer. Rounding off in Eq. (41) leads to noticeable steps in $f_{\text{top}}(p, \alpha)$ for smaller N .

We emphasize that by the help of Eqs. (44) and (45), one can find the exact expression for the topology function for arbitrary system sizes. Since it is a rather lengthy expression, we skip it in the text but we will use it in Fig. 4. Moreover, as can be seen in Fig. 4, a system size N of the order $O(100)$ is sufficient to obtain a dynamical behavior that is comparable with the thermodynamic limit. Further, the critical coupling strength \varkappa_c has been derived in the thermodynamic limit (see Eq. (40)). For this reason it is only consistent to calculate the topology function in the limit $N \rightarrow \infty$ as well.

B. Comparison of the Critical Coupling Strength; Simulations vs. Theory

In our simulations, the stochastic differential equations (1) are integrated up to $t = 600$ with time step $h = 0.05$ by using the Heun scheme [45]. The periods of the oscillators are $T \sim O(10)$, so our integrations cover $O(10)$ periods. Moreover, in order to calculate statistical equilibria, we discard the data up to $t = 200$, by which transient effects are safely avoided. The statistical equilibria are further calculated as averages over at least 100 different network realizations. We emphasize that all the different network configurations do not differ only in the configuration of the connections, but the oscillators on the network differ as well: all the natural frequencies and the initial values of the phases change from one configuration to another one.

Hong, Choi and Kim (2002) consider the Kuramoto model without noise on a small-world network, which is constructed according to the Watts-Strogatz model [43], where shortcuts are the result of rewiring the edges of the initial regular network with a certain probability p [21]. They calculate the order parameter averaged over time $\langle \dots \rangle$ and network realizations $[\dots]$ and use the following

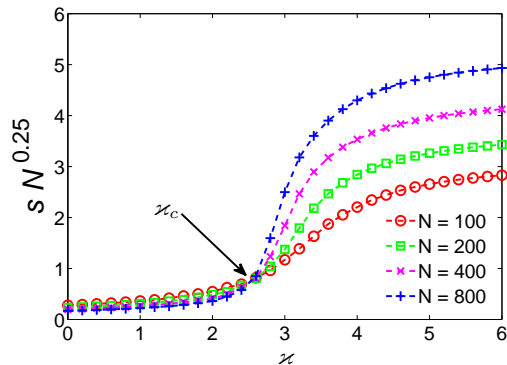


FIG. 5: (Color online) Numerical determination of critical coupling strength by plotting the order parameter s times $N^{0.25}$ for different system sizes in dependence on the coupling strength. According to Eq. (48) the intersection of the curves indicates the critical coupling strength. Parameter values here: $\alpha = 0.05$, $p = 0.1$, $D = 0.05$, $\sigma = 0.02$.

scaling form:

$$s := \left[\left\langle \left| \frac{1}{N} \sum_{j=1}^N e^{i\phi_j} \right| \right\rangle \right] = N^{-\frac{\beta}{\nu}} F \left[(\kappa - \kappa_c) N^{\frac{1}{\nu}} \right], \quad (48)$$

where $F[\cdot]$ is some scaling function. In particular it is found that β and ν have the same values as in the globally connected network, namely $\beta \approx \frac{1}{2}$ and $\nu \approx 2$.

The findings propose a finite-size scaling analysis to calculate the critical coupling strength, because at $\kappa = \kappa_c$ the function $F[\cdot]$ is independent of the system size N . By plotting $s \cdot N^{0.25}$ as a function of κ for various network sizes N , we can measure the critical coupling strength κ_c as a well-defined intersection point, see Fig. 5.

In order to compare the theory, expressed by the critical coupling strength (Eq. (40)), with simulations on the proposed dense small-world networks, we use as topology functional the approximation for large systems (cf. Eq. (46)).

In the following we further consider a Gaussian frequency distribution $g_{\text{gauss}}(\omega)$ with vanishing mean and standard deviation σ . Then for the diversity functional (39) the expression

$$f_{\text{div}}(D)[g_{\text{gauss}}] = 2\sqrt{\frac{2}{\pi}}\sigma \left[1 - \Phi \left(\frac{D}{\sqrt{2}\sigma} \right) \right]^{-1} e^{-\frac{1}{2}\frac{D^2}{\sigma^2}} \quad (49)$$

follows; $\Phi(\cdot)$ is the error function. The formula is equivalent to the mean field expression derived in [25] by means of an eigenvalue analysis. In appendix B we summarize the limiting cases of Eq. (49) and we give a comparison with other frequency distributions.

As can be seen in Figs. 6 and 7 we obtain a satisfying agreement for the critical coupling strength κ_c , regardless of whether we consider the dependencies on the topology (Fig. 6) or on the diversity (Fig. 7).

Especially for $p > 0.1$, $\alpha > 0.1$ or $\sigma < 0.5$ and for the dependency on the noise intensity D in general, we obtain almost a perfect agreement between theory and simulations. For smaller values of p or α there is a small discrepancy, but the shape of the curves can be well reproduced.

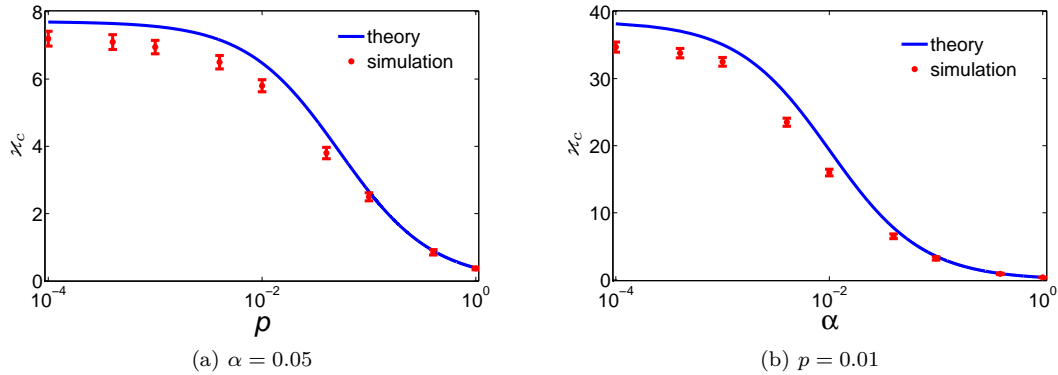


FIG. 6: (Color online) The dependencies of the critical coupling strength κ_c on the shortcut probability p and on the parameter α for the local connections are shown. Remaining parameters: $D = 0.05$, $\sigma = 0.2$.

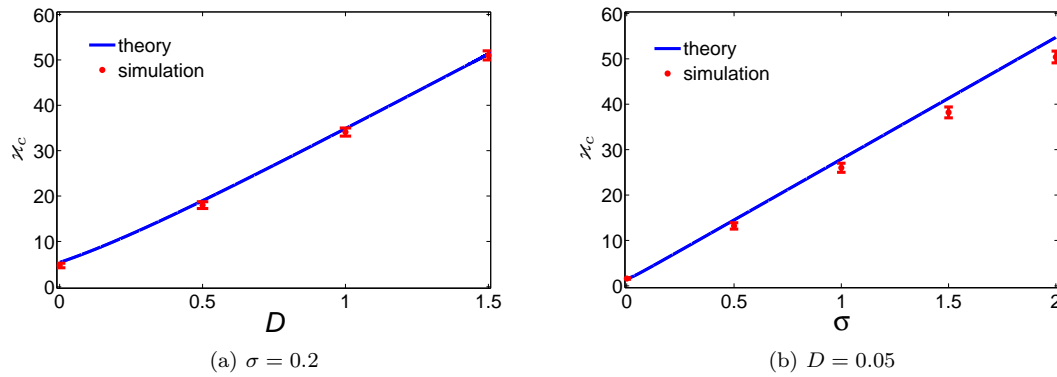


FIG. 7: (Color online) The dependencies of the critical coupling strength κ_c on the noise intensity D and on the diversity parameter σ are depicted. Remaining parameters: $\alpha = 0.05$, $p = 0.01$.

As expected, both weaker connectivity and larger diversity impede synchronization. Compare Eq. (47) and Tab. I for a summary of the limiting cases. In particular, for $p \rightarrow 0$ or $\alpha \rightarrow 0$ our results suggest a saturation at the values $\kappa_c = \frac{f_{\text{div}}(D)[g]}{\alpha}$ or $\kappa_c = \frac{f_{\text{div}}(D)[g]}{p}$, respectively.

Apparently, the weighted mean-field approximation tends to overestimate the critical coupling strength, which is counterintuitive, because the approximation corresponds to a weighted fully connected network and all-to-all connectivity should reduce the critical coupling strength. To see this, compare $p = 1$ or $\alpha = 1$ in Fig. 6, because both choices stand for all-to-all connectivity. So the coupling weights defined in Eq. (5) are able to mimic the original complexity in an overstated manner.

The disagreement for high standard deviations σ of the Gaussian frequency distribution seems to be analogous to the disagreement in the dependency on the topology, because in our derivation of the critical coupling strength, both the frequency distribution $g(\omega)$ and the degree distribution $P(k)$ are involved in averaging.

VII. BEYOND THE DENSE SMALL-WORLD NETWORKS

Since the mean-field description corresponds to all-to-all connectivity, we expect that the approximation loses validity in sparser networks. In order to effectively analyze the limitations, we consider separately Erdős-Rényi like random networks and regular networks. The first are constructed by assigning an edge probability of

$$p_e = p \cdot N^{q-1}, \quad 0 \leq p, q \leq 1 \quad (50)$$

for any two of the N nodes in the network. The only additional requirement is that besides the edge probability, each node connects a priori to another randomly chosen one. In this way we guarantee that there are no isolated nodes, which are not of interest here, because they are not able to take part in the synchronization process and only reduce the effective system size.

In the regular networks each node is coupled to the K next neighbors in both directions of the ring network and K is given by (compare Eq. (41))

$$K = \left\lfloor \frac{1}{2} [3 + \alpha \cdot (N - 4)^q] \right\rfloor, \quad 0 \leq \alpha, q \leq 1. \quad (51)$$

As for the random networks, we require that there are no isolated nodes, which is already implemented in the above choice ($K \geq 1$).

In both cases q is a denseness parameter, for $q = 1$ leads to dense and $q = 0$ to sparse networks [42].

We repeat the former analysis, see section VIB, with adjusting the normalization of the coupling, i.e., we substitute $N \rightarrow N^q$ in front of the coupling term (cf. Eq. (1)). Consequently, the topology functional becomes

$$f_{\text{top}}[P] = N^q \frac{\langle k \rangle}{\langle k^2 \rangle}. \quad (52)$$

In case of the regular networks it appears necessary to increase the system size for sparser networks in order to have distinguishable networks (see Eq. (51)), e.g. for $\alpha = 0.001$ and $q = 0.75$ we consider network sizes up to $N = 135000$. Again, $p = 10^{-4}$ and $\alpha = 10^{-4}$ are the smallest values considered in our numerical simulations.

In Fig. 8 the results are depicted. Unlike below the lines, we observe a mean-field synchronization transition above them. In particular, the markers correspond with the smallest p or α values for which we observe a synchronization transition with the critical mean-field exponents $\beta = \frac{1}{2}$ and $\nu = 2$ [21]. Those p and α values are denoted by p_{mf} or α_{mf} .

As expected, for sparser networks the mean-field approximation breaks down. Furthermore, it can be seen that random shortcuts favor the mean-field behavior, since we find the scaling relations $p_{\text{mf}} \sim 10^{-3q}$ and $\alpha_{\text{mf}} \sim 10^{-7q}$.

We also underline that our approach works, if the first two moments of the degree distribution exist. So, generally, scale-free networks that display a power-law decay $P(k) \sim k^{-\gamma}$ are excluded from our approximation. In [23] it was numerically shown that for $\gamma < 3$ the mean-field approach yields significant deviations. It is further analytically derived in [38] that only for $\gamma > 5$ the order parameter fulfills a finite-size scaling with the standard mean-field exponents, and for $2 < \gamma < 3$ the exponents depend on the degree exponent γ . Hence, more homogeneous degree distributions that can be characterized by the first two moments, favor the mean-field treatment as it was the case in our small-world example, see Fig. 3.

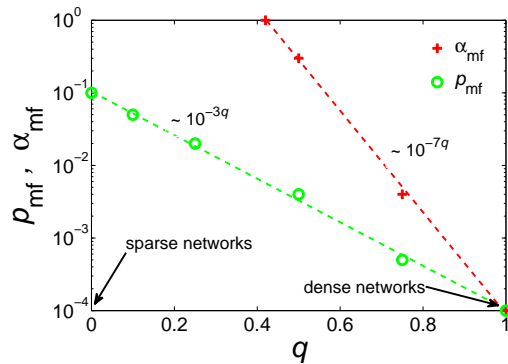


FIG. 8: (Color online) Smallest p (random network) and α (regular network) values for which a synchronization transition with the standard mean-field exponents can be observed, are shown as functions of the denseness parameter q . We denote these values by p_{mf} and α_{mf} . Dashed lines depict the scaling behaviors.

VIII. CONCLUSION

We have investigated noisy Kuramoto oscillators on undirected ring networks, whose complex structure is approximated by a weighted fully connected network. The weights are obtained by a specific combinatorial consideration of the connectivity, where the original network is considered to be random and uncorrelated. We have shown that this procedure leads to a weighted mean-field approximation, which enabled us to evaluate analytically the critical coupling strength κ_c that marks the onset of synchronization in the network. As a result, we have found that κ_c is a product of two functionals. The first one is a functional of the degree distribution and therefore depends solely on the network topology, while the second one is a functional of the frequency distribution and a function of the noise intensity.

As such, we have provided support for the previous separate consideration of network complexity and noise with regard to the Kuramoto model in the literature.

In order to compare the theory with simulations, we have investigated a dense small-world network model. As typical of small-world networks [44], we start with a regular network consisting only of next neighbor couplings, and then we randomly add shortcuts. In this way one can study the impact and the interplay of regular local edges and random shortcuts. We have found that in a large small-world network, regular local edges and random shortcuts play almost the same role.

Our dense small-world network model allows scaling between a locally and a globally connected network, which is well-suited for testing the mean-field approximation. In case of all-to-all connectivity the mean-field description is exact; by decreasing the connectivity we can determine the arising discrepancies between the original complexity and our estimate.

It has turned out that the analytical and the numerical results are consistent to each other in particular, finite-size scaling analysis with mean-field exponents always gives a well-defined intersection point. Hence, the extended Kuramoto model on dense small-world networks shows a mean-field synchronization transition.

We have completed our work by addressing further network models. There we have shown that random connections favor a mean-field approach in the sense that regular networks have to be more densely connected in order to yield a mean-field synchronization transition. Highly heterogeneous networks in which the mean-field description breaks down, have also been discussed.

Future work has to be done with regard to network complexity. For instance whether networks of higher dimension show significant qualitative differences. In particular, the problem of time-dependent coupling strengths or even time-dependent number of nodes and edges has to be tackled. A next step could also be the consideration of time delays in the coupling. Furthermore, network costs have to be taken into account, which should allow to evaluate the efficiency of a synchronization process.

Acknowledgments

This work was supported by GRK1589/1. We acknowledge F. Sagués, S. Martens and P. K. Radtke for a critical reading of the manuscript and useful comments.

Appendix A: Dense Small-World Networks

Here we provide numerical evidence for the existence of dense small-world networks, see Fig. 9. In order to do this, we have to compare such dense small-world networks with random networks. However, the random network used for the comparison must not have any isolated nodes. Otherwise path length and clustering coefficient are not (well) defined. We take as an almost random network (similar to Watts and Strogatz [43]) a network generated with our model, but with a minimum amount of coupled next neighbors, so we choose $K = 1$ or an equivalent α (cf. Eq. (41)). The comparison makes sense, only if the average degree $\langle k \rangle$ of both networks is the same, which requires choosing the following shortcut probability p' for the random network:

$$p' = \frac{2(K-1)}{N-3} + \frac{N-2K-1}{N-3}p. \quad (\text{A1})$$

p is the shortcut probability used for the dense small-world network.

Having in mind the defining properties of a small-world network: $L \gtrsim L_{\text{random}}$ and $C \gg C_{\text{random}}$ [43], we observe small-world networks for values of p around 10^{-3} . For smaller values of α , i.e., fewer coupled next neighbors, the defining properties are better fulfilled. If α is too large the network under consideration is no small-world network anymore.

Appendix B: Diversity Functional for Different Frequency Distributions

In what follows, we consider the diversity functional for different frequency distributions: uniform distribution $g_{\text{uni}}(\omega)$, identical oscillators $g_{\text{ident}}(\omega)$ and Lorentzian distribution $g_{\text{lorenz}}(\omega)$. We obtain the following expressions for the diversity functionals (cf. Eq. (39)):

$$\begin{aligned} f_{\text{div}}(D)[g_{\text{uni}}] &= 2\sqrt{3}\sigma \left[\arctan \left(\frac{\sqrt{3}\sigma}{D} \right) \right]^{-1}, \\ f_{\text{div}}(D)[g_{\text{ident}}] &= 2D, \\ f_{\text{div}}(D)[g_{\text{lorenz}}] &= 2(D + \gamma). \end{aligned} \quad (\text{B1})$$

σ and γ are the standard deviation and the scale parameter, respectively, while D gives the noise intensity. In Fig. 10 the dependencies on D , σ or γ are depicted. We observe a greater

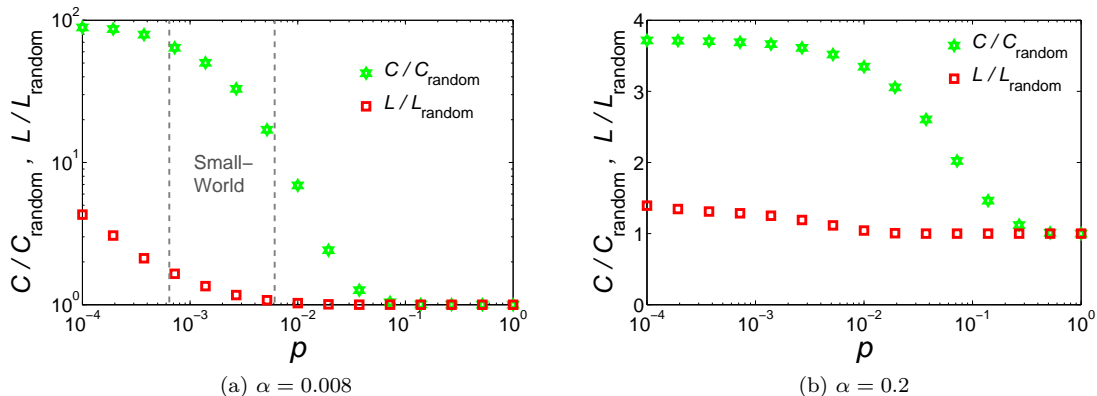


FIG. 9: (Color online) Numerically calculated average path lengths L and clustering coefficients C as a function of shortcut probability p for a network of 501 nodes. The radius of coupled next neighbors (compare Eq. (41)) equals $K = 2$ (Fig. 9(a)) or $K = 50$ (Fig. 9(b)), respectively. Dashed lines indicate the area, in which our model generates a small-world network.

difference in the dependency on diversity than on noise. In particular, for large values of D , all the different diversity functionals show the same linear dependency on D (cf. Fig. 10(a)). In case of Gaussian, uniformly and identically distributed natural frequencies ω , it can be shown that the diversity functional even approaches the same line for $D \rightarrow \infty$.

However, the above observation is not surprising, because the noise acts on the natural frequencies. So if the noise intensity D is very high, it makes almost no difference how the natural frequencies are distributed, because the diversity of the oscillators mainly comes from the random fluctuations induced by the noise.

Instead, for $D = \text{const.}$ and increasing diversity parameter σ or γ , the different nature of the various frequency distributions manifests more and more in a different synchronizability (cf. Fig. 10(b)). Especially the comparison between the uniform and the Lorentzian distribution for the same σ and γ values is interesting. In terms of synchronizability we observe that for lower diversity the uniform frequency distribution is more favorable than the Lorentzian distribution, while for higher diversity the Lorentzian distribution is more favorable.

Of course, vanishing diversity, i.e., $\sigma \rightarrow 0$ or $\gamma \rightarrow 0$, results in identical oscillators, so that the diversity functional approaches the same value for every frequency distribution. In Tab. I we summarize these results.

LIMITING CASE	$D \ll 1$	$\sigma \ll 1$	$D \gg 1$	$\sigma \gg 1$
$f_{\text{div}}(D)[g_{\text{gauss}}]$	$2\sqrt{\frac{2}{\pi}}\sigma + \frac{4}{\pi}D + O(D^2)$	$2D + \frac{2}{D}\sigma^2 + O(\sigma^4)$	$2D + O(\frac{1}{D})$	$2\sqrt{\frac{2}{\pi}}\sigma + O(1)$
$f_{\text{div}}(D)[g_{\text{uni}}]$	$\frac{4\sqrt{3}}{\pi}\sigma + \frac{8}{\pi^2}D + O(D^2)$	$2D + \frac{2}{D}\sigma^2 + O(\sigma^4)$	$2D + O(\frac{1}{D})$	$\frac{4\sqrt{3}}{\pi}\sigma + O(1)$
$f_{\text{div}}(D)[g_{\text{ident}}]$	$2D$	$2D$	$2D$	$2D$
$f_{\text{div}}(D)[g_{\text{lorentz}}]$	$2\sigma + 2D$	$2D + 2\sigma$	$2D + O(1)$	$2\sigma + O(1)$

TABLE I: The limiting cases of the diversity functional for different frequency distributions. Here $\sigma = \lambda$.

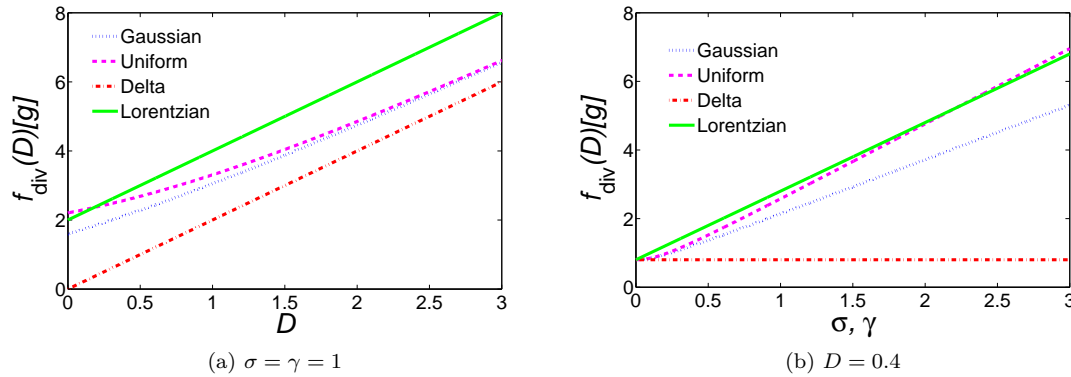


FIG. 10: (Color online) The diversity functional for different frequency distributions as a function of noise intensity D , standard deviation σ or scale parameter γ .

-
- [1] R. Roy and Jr. K. S. Thornburg. *Phys. Rev. Lett.*, 72(13):2009–2012, 1994.
 - [2] J. Buck and E. Buck. *Sci. Am.*, 234:74–85, 1976.
 - [3] J. Dye. *J. Comp. Physiol. A*, 168(5):521–532, 1991.
 - [4] T. A. Engel, B. Helbig, D. F. Russell, L. Schimansky-Geier, and A. B. Neiman. *Phys. Rev. E*, 80(021919):1–7, 2009.
 - [5] S. Olmi, R. Livi, A. Politi, and A. Torcini. *Phys. Rev. E*, 81(046119):1–7, 2010.
 - [6] S. Luccioli and A. Politi. *Phys. Rev. Lett.*, 105(158104):1–4, 2010.
 - [7] T. Doerr, R. Denger, and W. Trautwein. *Pflug. Arch. Eur. J. Phys.*, 413(6):599–603, 1989.
 - [8] M. K. McClintock. *Nature*, 229:244–245, 1971.
 - [9] H. C. Wilson. *Psychoneuroendocrino.*, 17(6):565–591, 1992.
 - [10] Z. Yang and J. C. Schank. *Human Nature*, 17(4):433–447, 2006.
 - [11] A. Pikovsky, M. Rosenblum, and J. Kurths. *Synchronization: A universal concept in nonlinear sciences*. Cambridge Univ. Press, U. K., 2003.
 - [12] P. Tass. *Phase Resetting in Medicine and Biology*. Springer-Verlag, Berlin, Heidelberg, New York, Tokyo, 2007.
 - [13] V. S. Anishchenko, V. Astakhov, A. Neiman, T. Vadisova, and L. Schimansky-Geier. *Nonlinear Dynamics of Chaotic and Stochastic Systems*. Springer-Verlag, Berlin, Heidelberg, New York, Tokyo, 2007.
 - [14] A. Balanov, N. Janson, D. Postnov, and O. Sosnovtseva. *Synchronization: From Simple to Complex*. Springer-Verlag, Berlin, Heidelberg, New York, Tokyo, 2010.
 - [15] B. Lindner, J. García-Ojalvo, A. Neiman, and L. Schimansky-Geier. *Phys. Rep.*, 392:321–424, 2004.
 - [16] A. T. Winfree. *J. Theor. Biol.*, 16:15–42, 1967.
 - [17] Y. Kuramoto. Self-entrainment of a population of coupled non-linear oscillators. In H. Araki, editor, *Lect. Notes Phys.*, volume 39, pages 420–422. Springer, New York, 1975.
 - [18] Y. Kuramoto. *Chemical Oscillations, Waves, and Turbulence*. Springer-Verlag, Berlin, Heidelberg, New York, Tokyo, 1984.
 - [19] J. Ochab and P. F. Góra. *Acta Phys. Pol. B Proceedings Supplement*, 3(2):453–462, 2010.
 - [20] O. Sporns, D. R. Chialvo, M. Kaiser, and C. C. Hilgetag. *TRENDS Cogn. Sci.*, 8(9):418–425, 2004.
 - [21] H. Hong, M. Y. Choi, and B. J. Kim. *Phys. Rev. E*, 65(026139):1–5, 2002.
 - [22] T. Ichinomiya. *Phys. Rev. E*, 70(026116):1–5, 2004.

- [23] J. G. Restrepo, E. Ott, and B. R. Hunt. *Phys. Rev. E*, 71(036151):1–12, 2005.
- [24] H. Sakaguchi. *Prog. Theor. Phys.*, 79(1):39–46, 1988.
- [25] S. H. Strogatz and R. E. Mirollo. *J. Stat. Phys.*, 63(3/4):613–635, 1991.
- [26] M. A. Zaks, A. B. Neiman, S. Feistel, and L. Schimansky-Geier. *Phys. Rev. E*, 68(066206):1–9, 2003.
- [27] R. Albert and A.-L. Barabási. *Rev. Mod. Phys.*, 74(1):47–97, 2002.
- [28] M. E. J. Newman. *SIAM Rev.*, 45(2):167–256, 2003.
- [29] S. Boccaletti, V. Latora, Y. Moreno, M. Chavez, and D.-U. Hwang. *Phys. Rep.*, 424:175–308, 2006.
- [30] A. Arenas, A. Díaz-Guilera, J. Kurths, Y. Moreno, and C. Zhou. *Phys. Rep.*, 469:93–153, 2008.
- [31] S. H. Strogatz. *Physica D*, 143:1–20, 2000.
- [32] E. Ott. *Chaos in Dynamical Systems*. Cambridge Univ. Press, U. K., 2002.
- [33] J. A. Acebrón, L. L. Bonilla, C. J. Pérez Vicente, F. Ritort, and R. Spigler. *Rev. Mod. Phys.*, 77:137–185, 2005.
- [34] C. W. Wu. *Synchronization in Complex Networks of Nonlinear Dynamical Systems*. World Scientific, 2007.
- [35] A. Barrat, M. Barthélemy, and A. Vespignani. *Dynamical Processes on Complex Networks*. Cambridge Univ. Press, U. K., 2008.
- [36] H. Hong and S. H. Strogatz. *Phys. Rev. E*, 84(046202):1–6, 2011.
- [37] J. D. Crawford and K. T. R. Davies. *Physica D*, 125:1–46, 1999.
- [38] D.-S. Lee. *Phys. Rev. E*, 72(026208):1–6, 2005.
- [39] H. E. Stanley. *Introduction to Phase Transitions and Critical Phenomena*. Oxford University Press, New York, 1971.
- [40] R. E. Mirollo and S. H. Strogatz. *J. Stat. Phys.*, 60(1/2):245–261, 1990.
- [41] B. Sonnenschein, L. Schimansky-Geier, and F. Sagués. *In preparation*.
- [42] B. R. Preiss. *Data Structures and Algorithms with Object-Oriented Design Patterns in C++*. Wiley & Sons, 1998.
- [43] D. J. Watts and S. H. Strogatz. *Nature*, 393:440–442, 1998.
- [44] M. E. J. Newman and D. J. Watts. *Phys. Rev. E*, 60(6):7332–7342, 1999.
- [45] R. Mannella. A Gentle Introduction to the Integration of Stochastic Differential Equations. In J. A. Freund and T. Pöschel, editors, *Stochastic Processes in Physics, Chemistry, and Biology*, volume 557, pages 353–364. Springer-Verlag, Berlin Heidelberg, 2000.